Metal-Insulator-Semiconductor Anodes for Ultrastable and Site-Selective Upconversion Photoinduced Electrochemiluminescence

Yiran Zhao, Julie Descamps, Soraya Ababou-Girard, Jean-Francois Bergamini, Lionel Santinacci, Yoan Léger, Neso Sojic, Gabriel Loget

Metal-Insulator-Semiconductor Anodes for Ultrastable and Site-Selective Upconversion Photoinduced Electrochemiluminescence

Yiran Zhao,[a] Julie Descamps,[b] Soraya Ababou-Girard,[c] Jean-François Bergamini,[a] Lionel Santinacci,[d] Yoan Léger,*[e] Neso Sojic,*[b] Gabriel Loget*[a]

[a] Y. Zhao, Dr. J.-F. Bergamini, Dr. G. Loget
Univ Rennes, CNRS, ISCR (Institut des Sciences Chimiques de Rennes)-UMR6226
Rennes F-35000, France.
E-mail: gabriel.loget@univ-rennes1.fr
[b] J. Descamps, Prof. N. Sojic
University of Bordeaux, Bordeaux INP, ISM, UMR CNRS 5255
Pessac 33607, France.
E-mail: neso.sojic@enscbp.fr
[c] Prof. S. Ababou-Girard
Univ Rennes, CNRS, IPR (Institut de Physique de Rennes)-UMR 6251
F-35000 Rennes, France.
[d] Dr. L. Santinacci
Aix-Marseille Univ, CNRS, CINaM,
Marseille, France.
[e] Dr. Y. Léger
Univ Rennes, INSA Rennes, CNRS, Institut FOTON-UMR 6082
F-35000, Rennes, France.
E-mail: yoan.leger@insa-rennes.fr

Abstract: Photoinduced electrochemiluminescence (PECL) allows the electrochemically assisted conversion of low-energy photons into high-energy photons at an electrode surface. This concept is expected to have important implications, however, it is dramatically limited by the stability of the surface, impeding future developments. Here, a series of metal-insulator-semiconductor junctions, using photoactive *n*-type Si (*n*-Si) as a light absorber covered by a few-nanometer-thick protective SiO_x/metal (SiO_x/M, with M = Ru, Pt, and Ir) overlayers are investigated for upconversion PECL of the model co-reactant system involving the simultaneous oxidation of tris(bipyridine)ruthenium(II) and tri-n-propylamine. We show that *n*-Si/SiO_x/Pt and *n*-Si/SiO_x/Ir exhibit high photovoltages and record stabilities in operation (35 h for *n*-Si/SiO_x/Ir) for the generation of intense PECL with an anti-Stokes shift of 218 nm. We also demonstrate that these surfaces can be employed for spatially localized PECL. These unprecedented performances are extremely promising for future applications of PECL.

Introduction

Photoinduced electrochemiluminescence (PECL) is a growing field of research that combines charge transfer at the semiconductor/electrolyte interface and electrochemiluminescence (ECL).[1–6] ECL is a well-known phenomenon that involves an electrochemical reaction generating the excited state of a luminophore at an electrode surface leading to light emission.[7,8] A model ECL system that has become widely used in medical diagnosis[9,10] and currently attracts considerable attention for sensing,[11–13] imaging,[14–17] and microscopy,[18–22] involves the simultaneous oxidation of tris(bipyridine)ruthenium(II) ($[Ru(bpy)_3]^{2+}$) and tri-n-propylamine (TPrA) in an aqueous electrolyte at physiological pH. In PECL, this co-reactant ECL system can be employed with Si photoanodes to perform an electrochemically-assisted upconversion process[3] where the absorption of infrared (IR) photons (>800 nm) results in the emission of visible photons (632 nm) at the electrode vicinity, as shown in Figure 1a. Another remarkable aspect of PECL is the considerable decrease of the ECL onset potential, which is caused by the photovoltage at the semiconductor interface and allows for triggering photon emission at record low potentials[3–5] even if ECL reactions are always highly exergonic and typically require the application of high potentials.[23,24] PECL systems are extremely promising for ultrasensitive detection, microscopy, light-addressable devices, and IR imaging.[1–6] However, as for all photoelectrochemical processes, they are strongly limited by the poor stability of the photoelectrode.[25] The advantages of PECL and the challenges in this field have been discussed in a recent review.[26] So far, upconversion PECL could be demonstrated in water and was reported for short durations, typically in the minute scale (Table S1) for Si-based photoanodes protected with a covalently-attached organic monolayer,[4],[27] and *n*-Si/SiO_x/Ni metal-insulator-semiconductor (MIS) photoanodes.[3] These operation times are obviously too short to allow a prospect of practical application. A possible solution to this bottleneck is the use of oxide-based photoanodes, known to exhibit higher stabilities. This strategy, which has been recently explored with $BiVO_4$[5] and α-Fe_2O_3,[6] resulted in considerably improved PECL stability of 2 h (Table S1).[5]

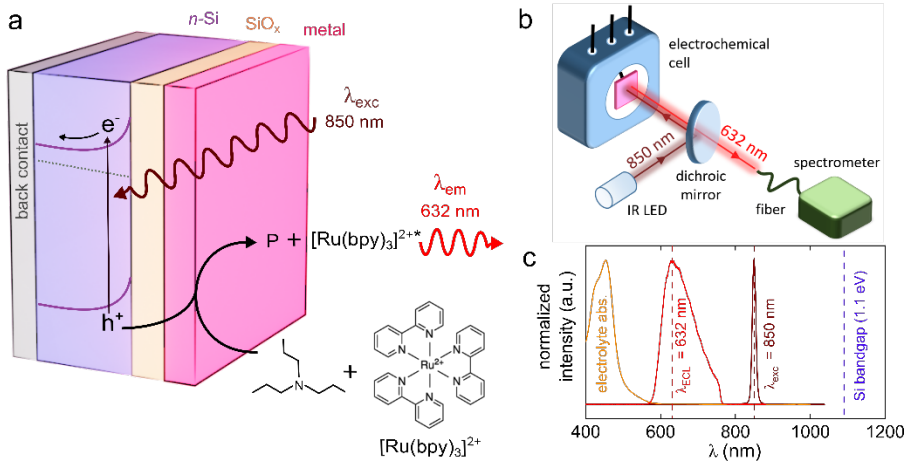

Figure 1. Upconversion PECL and MIS structures. a) Scheme showing the photoinduced charge transfer process occurring at the MIS photoanode initiated by the absorption of IR light (λ_{exc}) and leading to the emission of visible light (λ_{em}) by PECL (the side product of the TPrA radicals formed during the ECL process is denoted by P). b) Scheme of the photoelectrochemical setup employed for studying PECL. c) Normalized spectra of the electrolyte absorption (orange curve), emission of the LED used in this work (brown), PECL emission (red curve), and bandgap position of Si (blue dashed line).

However, the wide bandgaps of oxide-based semiconductors do not allow absorption of low-energy photons and strictly prohibit their use in upconversion PECL processes (allowing only Stokes-type PECL).[5,6] Consequently, future developments in upconversion PECL crucially rely on the development of stable narrow-bandgap photoanodes.

Silicon is established as the material of choice in many light-conversion applications due to its abundancy, nontoxicity, and narrow bandgap (E_g = 1.1 eV) which makes it active from IR to UV regions. For these reasons, it is undeniably the most important semiconductor in the photovoltaic industry,[28,29] a highly promising material for photonics,[30,31] and a prime candidate for photoelectrochemical devices.[32–34] However, manufacturing stable Si photoelectrodes is still a major challenge[35],[36] because of its low intrinsic activity and poor stability in aqueous solutions.[37] This issue is even more pronounced on photoanodes as photocorrosion generates an electrically insulating SiO_x layer that inhibits charge transfer at the solid/electrolyte interface. In this respect, Si photoanodes based on the MIS junction, a key architecture of modern electronics, are attracting considerable attention because of their remarkable properties.[38–45] Specifically, it has been reported that MIS photoanodes made on *n*-type Si (*n*-Si) wafers can be used to efficiently and durably oxidize water in harsh conditions.[46–52]

In typical MIS photoanodes, the metal thin film is a key element that must have a thickness in the nanometer range to enable light transmission that ensures electron/hole (e^-/h^+) pair photogeneration in the semiconductor.[35–49] Besides, it plays a crucial role by *i*) protecting the semiconductor by avoiding its corrosion,[35–37] *ii*) ensuring the efficient collection of charge carriers through the insulator tunnel layer,[38,39] *iii*) granting fast kinetics of the electrochemical reaction,[53] and *iv*) ensuring a high barrier Schottky junction to promote high photovoltage.[41,54] In this article, we report on our investigations of three Si/SiO_x/metal (Si/SiO_x/M, with M = Ru, Pt, and Ir) MIS electrodes for the upconversion PECL of the $[Ru(bpy)_3]^{2+}$/(TPrA) model system. Ru, Pt, and Ir were chosen as potential candidates because, according to their Pourbaix diagrams, they are expected to exhibit higher stability[55] in PECL conditions (pH = 7.4) than the previously-used Ni thin films.[3] In addition, these metals are known for their good electrocatalytic activities and possess high work functions (4.7 eV < W_M < 5.9 eV),[56,57] essential for creating a photoactive junction with *n*-Si and producing high photovoltages.[54] Our results demonstrate that, while Si/SiO_x/Ru fails in promoting PECL, *n*-Si/SiO_x/Pt and *n*-Si/SiO_x/Ir photoelectrodes exhibit unprecedented performances, enabling long-term PECL generation with ultrathin film thicknesses (3 nm), opening exciting opportunities for PECL.

Results and Discussion

Preparation and characterization of the surfaces

The Si/SiO_x/M MIS junctions were prepared, first, by chemically oxidizing cleaned Si (100) wafers to create a 1.5-to-2 nm-thick SiO_x tunnel layer, as we previously reported.[50,58] After that, a 3 nm-thick metal layer was deposited on SiO_x by direct current magnetron sputtering onto 1.5x1.5 cm² Si/SiO_x surfaces. During deposition, the thickness of the coating was monitored *in-situ* using a quartz crystal microbalance (QCM) and monitored *ex-situ* by atomic force microscopy (AFM). This low thickness value was specifically chosen because previous research in the field of Si-based MIS anodes has revealed that ultralow metal thicknesses (< 5 nm) promote the highest photoelectrochemical performance.[3,40,47]

AFM and scanning electron microscopy (SEM) were performed on the so-prepared Si/SiO_x/M surfaces and revealed high uniformity and planarity of the metal films, which is demonstrated by the absence of observable features on the high-magnification SEM pictures of Figure S1 and the low root mean square (RMS) roughness values of 0.36, 0.28, and 0.33 nm determined from the AFM pictures of Si/SiO_x/Ru, Si/SiO_x/Pt, and Si/SiO_x/Ir presented in Figure 2a,b, and Figure S2. The composition of the outermost surface of the electrodes was analyzed by X-ray photoelectron spectroscopy (XPS), as shown in Figure 2c. The grey spectrum, measured for Si/SiO_x, indicates that, before deposition, the surface is only constituted of Si and O atoms, with a low content of adventitious carbon. The colored spectra, acquired after the deposition of the metal thin films, confirm the presence of the deposited metals with characteristic Pt 4f peaks at 71.5 and 74.9

eV, Ru 3d peak at 280.5 and 284.6 eV, and Ir 4f peaks at 61.0 and 63.9 eV. These spectra also feature a strong disappearance of the Si 2s and 2p peaks, which is in good agreement with dense and conformal metal thin films. The presence of oxygen, which can be observed by its 1s peak localized between 530 and 534 eV, originates from the native oxide/hydroxide phase at each metal surface and the underlying SiO_x layer.

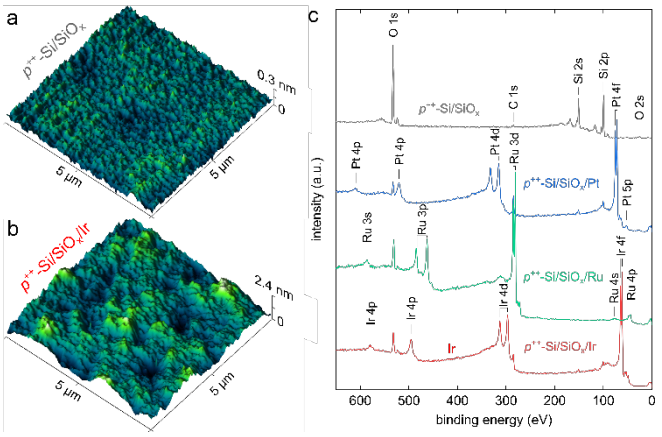

Figure 2. Characterization of the MIS surfaces. a,b) AFM pictures of the p^{++}-Si/SiO_x surface before coating (a), and p^{++}-Si/SiO_x/Ir after Ir coating (b). c) XPS spectra of the p^{++}-Si/SiO_x surface before coating (grey) and the p^{++}-Si/SiO_x/M surfaces with M = Pt (blue), M = Ru (green), and M = Ir (red).

Electrochemiluminescence (ECL)

The junctions were then investigated for ECL of the co-reactant $[Ru(bpy)_3]^{2+}$/TPrA system. In the first experiments, the MIS electrodes were manufactured onto degenerate p^{++}-Si. This type of silicon, characterized by a high concentration of dopants and low resistivity (ρ = 0.001 - 0.005 Ω cm), is non-photoactive, which allows straightforward assessment of the ECL performance for each MIS electrode in the dark. The effects of the ECL reagents dissolved in phosphate-buffered saline (PBS) were investigated on p^{++}-Si/SiO_x/Ir. Figure 3a presents the cyclic voltammograms (CVs, top panel) and the corresponding ECL intensity vs potential curves (bottom panel). This figure shows that, when studied individually, TPrA (black curves) and $[Ru(bpy)_3]^{2+}$ (blue curves) are oxidized at potentials higher than 0.9 V and 1 V, respectively (all potentials reported in this article are referred vs Ag/AgCl (3 M KCl)), and do not emit detectable ECL. However, when they are present together in the electrolyte, their concomitant oxidation produces ECL from 1 V, showing the suitability of the p^{++}-Si/SiO_x/Ir anode for triggering $[Ru(bpy)_3]^{2+}$/TPrA ECL.

Next, the effect of the metal thin film was investigated. The electrochemical and corresponding ECL responses for the three p^{++}-Si/SiO_x/M anodes in the ECL electrolyte (100 mM TPrA and 5 mM $[Ru(bpy)_3]^{2+}$ in PBS) are presented in Figure 3b. Here, we can observe a strong similarity between p^{++}-Si/SiO_x/Ir (red curves) and p^{++}-Si/SiO_x/Pt (blue curves) that both granted ECL emission from 1 V and stable voltammograms. However, p^{++}-Si/SiO_x/Ru exhibited a completely different behavior. First, it only produced measurable ECL at potentials higher than 1.35 V (detailed data for this anode is presented in Figure S3) and its CV features changed drastically during cycling. The first cycle, shown as a thin green line in Figure 3b, exhibits a large oxidation wave with a current density (j) as high as 8.7 mA cm^{-2}, while subsequent cycles are associated with smaller values (j <1.7 mA cm^{-2}) and decaying ECL intensity (Figure S3). Similar behavior was observed in the absence of the ECL reagents (in an electrolyte consisting only of PBS, Figure S4a), which suggests that the large current observed during the first forward scan is mainly caused by the oxidation of the Ru thin film and the oxidation of water. The higher ECL onset potential is attributed to the low activity of this anode and the evolution of the CVs during cycling is consistent with strong damage of the Ru thin film during the first cycle, leading to its deactivation. This is in good agreement with the AFM measurements presented in Figure S4c, which shows a considerable increase in the surface roughness after the CV study.

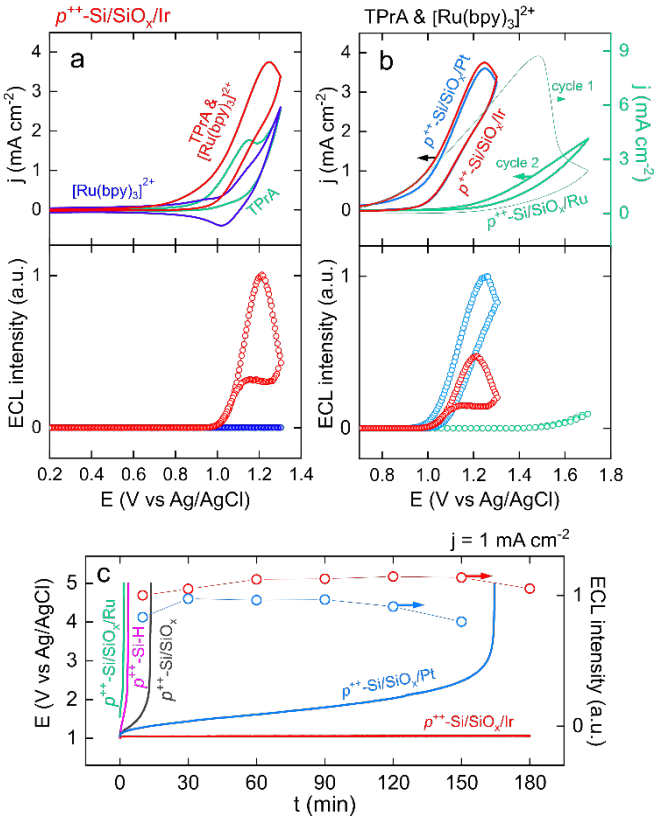

Figure 3. ECL at non-photoactive MIS electrodes. a) CVs measured in the dark (top) and corresponding ECL intensity profiles (bottom) measured on p^{++}-Si/SiO_x/Ir in the presence of 100 mM TPrA (green), 5 mM $[Ru(bpy)_3]^{2+}$ (purple), and 100 mM TPrA + 5 mM $[Ru(bpy)_3]^{2+}$ (red). b) CVs measured in the dark (top) and corresponding ECL intensity profiles (bottom) measured in the presence of 100 mM TPrA + 5 mM $[Ru(bpy)_3]^{2+}$ on p^{++}-Si/SiO_x/Ir (red), p^{++}-Si/SiO_x/Pt (blue), and p^{++}-Si/SiO_x/Ru (green). The first cycle measured on p^{++}-Si/SiO_x/Ru is shown by a thin green line. The ECL intensity shown for p^{++}-Si/SiO_x/Ru corresponds to the second CV cycle. c) CP curves (lines) recorded at 1 mA cm^{-2} on p^{++}-Si/SiO_x/Ru (green), p^{++}-Si-H (pink), p^{++}-Si/SiO_x (black), p^{++}-Si/SiO_x/Pt (blue), and p^{++}-Si/SiO_x/Ir (red). The ECL intensity is shown by circles for p^{++}-Si/SiO_x/Pt (blue circles) and p^{++}-Si/SiO_x/Ir (red circles). These experiments were performed in PBS (pH 7.4), CVs were recorded at 50 mV s^{-1}.

The stability was assessed by galvanostatic experiments in which a current density of 1 mA cm^{-2} was applied and the anode potential was monitored. In these tests, the electrolyte was circulated in the cell using a peristaltic pump (flow rate = 0.7 mL s^{-1}), which ensures efficient mass transport of the ECL reactants at the solid/liquid interface leading to homogenous and brighter

ECL emission for a long duration.[59] The chronoamperograms (CPs) of Figure 3c shows that freshly hydrogenated p^{++}-Si (p^{++}-Si-H, pink), uncoated p^{++}-Si/SiO$_x$ (grey), and p^{++}-Si/SiO$_x$/Ru (green) rapidly failed. It is evidenced by the strong potential increase (resulting from the degradation of the electrode interface) occurring a few minutes after the beginning of the test. Compared to these anodes, p^{++}-Si/SiO$_x$/Pt exhibited a considerable stability improvement and operated at a potential lower than 2 V for almost 2 h. However, after 160 min, its degradation led to a dramatic potential increase. Conversely, p^{++}-Si/SiO$_x$/Ir outperformed all studied anodes and could be used for 3 h without potential variation. In these conditions, p^{++}-Si/SiO$_x$/Ir and p^{++}-Si/SiO$_x$/Pt produced a bright ECL emission during the entire experiment (circles in Figure 3c) that was visible with naked eyes.

Photoinduced electrochemiluminescence (PECL)

After having identified the best interfaces for ECL, we tested them for PECL. For that, MIS structures were prepared on moderately doped *n*-Si (ρ = 0.3-0.7 Ω cm) to yield photoactive *n*-Si/SiO$_x$/Pt and *n*-Si/SiO$_x$/Ir anodes (i.e., photoanodes). The typical emission responses obtained for ECL with a non-photoactive MIS surface and PECL for its photoactive equivalent can be compared in Figure 4a. This 3D plot presents the emission spectra as a function of potential recorded: *i*) in the dark on a non-photoactive p^{++}-Si/SiO$_x$/Ir producing ECL (left) and *ii*) under 850 nm illumination on a *n*-Si/SiO$_x$/Ir producing PECL (right). We now discuss the characteristic PECL features of the *n*-Si/SiO$_x$/M photoanodes.

In the CV (top part) of Figure 4b, it can be observed that both *n*-Si/SiO$_x$/Pt and *n*-Si/SiO$_x$/Ir are inactive in the dark, revealing their rectifying nature. However, when illuminated with λ_{exc} = 850 nm they afford photocurrents and PECL. While both non-photoactive anodes (p^{++}-Si/SiO$_x$/Ir and p^{++}-Si/SiO$_x$/Pt) triggered ECL at similar onset potential (*vide supra*, Figure 3b), the photoelectrochemical data presented in Figure 4b reveals that both photoanodes generates PECL at distinct potentials, which is characteristic of a different photovoltage (V_{oc}) at each photoactive MIS junctions. Subtraction of the onset potential values of ECL (p^{++}-Si/SiO$_x$/M in the dark) with that of PECL (illuminated *n*-Si/SiO$_x$/M) gives V_{oc} values of 485 and 280 mV for *n*-Si/SiO$_x$/Pt and *n*-Si/SiO$_x$/Ir photoanodes, respectively (arrows in Figure 4b). Remarkably, the photovoltage for *n*-Si/SiO$_x$/Pt corresponds to state-of-the-art performance for *n*-Si-based photoanodes[38,41,50] and is higher than that reported for *n*-Si/SiO$_x$/Ni (V_{oc} = 410 mV) in similar conditions.[3] V_{oc} values are correlated with the Schottky barrier height of the MIS device, which is theoretically controlled by the work function of the metal (Figure S5). However, in practice, the effective Shottky barrier height is also strongly affected by other parameters such as the interface quality and homogeneity.[54] If Ir and Pt have reported W_M values lying in the same range (5.1 eV < W_M < 5.9 eV),[56,57] in our case, Pt produces a higher Schottky barrier at *n*-Si/SiO$_x$. This finding is well in line with a recent work where 2 nm-thick Pt thin films were employed as Schottky contact to considerably enhance the photovoltage of *n*-Si-based MIS photoanodes for water splitting.[41] In this regard, it is also known that the thickness of the metal thin film often affects photovoltage on MIS photoanodes, which we experimentally verified for *n*-Si/SiO$_x$/Ir, as shown in Figure S6.

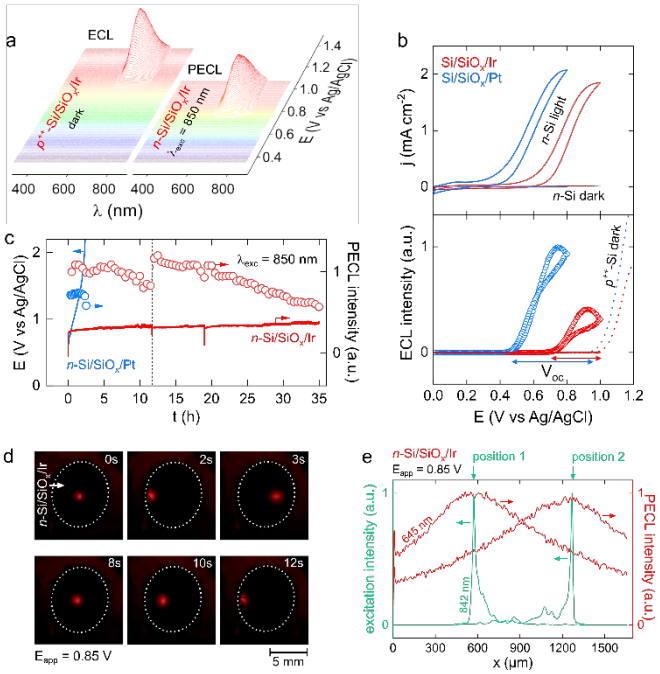

Figure 4. PECL at photoactive MIS electrodes. a) Consecutive ECL emission spectra recorded in the dark on p^{++}-Si/SiO$_x$/Ir (left) and illuminated *n*-Si/SiO$_x$/Ir (right) during linear sweep voltammetry. b) CVs (top) measured on *n*-Si/SiO$_x$/Ir (red) and *n*-Si/SiO$_x$/Pt (blue) in the dark and under 850 nm illumination. Corresponding PECL intensity profiles (bottom) measured on *n*-Si/SiO$_x$/Ir (red) and *n*-Si/SiO$_x$/Pt (blue) in the dark (full lines) and under 850 nm illumination (circles). The ECL measured in the dark on p^{++}-Si/SiO$_x$/Ir (red) and p^{++}-Si/SiO$_x$/Pt (blue) is also shown by dotted lines. c) CP curves (lines) recorded at 1 mA cm^{-2} on *n*-Si/SiO$_x$/Pt (blue), and *n*-Si/SiO$_x$/Ir (red) under 850 nm illumination. PECL intensity is shown by circles. The electrolyte was replaced at the time indicated by dashed vertical lines. d) Optical images showing the displacement of the PECL spot on *n*-Si/SiO$_x$/Ir by moving an 840 nm laser beam on that surface when a potential of 0.85 V is imposed, the white dashed line indicates the boundary of the electrode surface. These images were extracted from the movie available in the Supplementary file. e) Normalized intensity profile of the IR excitation pattern (green) and the PECL emission pattern (red) recorded at two different positions. This data was measured in the presence of 100 mM TPrA + 5 mM $[Ru(bpy)_3]^{2+}$ in PBS (pH 7.4), CVs were recorded at 50 mV s^{-1}.

Long-term stability was tested for both photoanodes at a photocurrent density of 1 mA cm^{-2} in the same conditions as that previously described, except that, in this case, the entire electrode surface was homogeneously illuminated at 850 nm. As presented in Figure 4c, *n*-Si/SiO$_x$/Pt exhibited a stability profile very close to that previously determined for its p^{++}-Si-based counterpart (both CP curves are plotted in Figure S7). The photoanode operated below 2 V for 140 min, then, a strong increase of its potential followed. Comparatively, *n*-Si/SiO$_x$/Ir exhibited exceptional stability and generated strong PECL over 35 h of operation with a minimal potential increase (red curve in Figure 4c). At the end of the test, the photoanode was still operating at a potential of 0.95 V, with a PECL intensity of 60% of the initial value, demonstrating the outstanding performance of *n*-Si/SiO$_x$/Ir. Four independently prepared *n*-Si/SiO$_x$/Ir were tested for at least 6 h and all promoted PECL identically, without noticeable performance decrease. After the stability test, the surface of *n*-Si/SiO$_x$/Ir was analyzed *ex-situ* by XPS (Figure S8) that revealed strong Ir 4f and 4d bands and weak Si 2s and 2p bands, demonstrating that the Ir film was still present and densely covered the Si/SiO$_x$ surface. An increase of the O 1s peak can also be noticed on the spectrum, which is

correlated with the oxidation of the surface during the photoelectrochemical experiment. Finally, AFM analysis performed on this surface (Figure S9) showed the apparition of bigger particles which may be correlated with the precipitation of insoluble species onto the photoanode, in good agreement with the increase of the carbon content observed on the XPS spectrum and the decrease of PECL intensity (Figure 4c). These results demonstrate that Pt and Ir thin films allow the promotion of upconversion PECL in water with record stabilities. So far, this phenomenon was only reported for 15 min[3] (Table S1), while our results show that *n*-Si/SiO_x/Pt and especially *n*-Si/SiO_x/Ir allow promoting PECL for tens of hours without any surface regeneration or re-activation treatments, as usually performed in classic ECL imaging or bioassays.[9,60] This remarkable emission stability opens new technological perspectives.

Finally, the most promising surface, namely, *n*-Si/SiO_x/Ir was tested for site-selective upconversion in proof-of-principle experiments. For that, the setup of Figure 1b was adapted for an 840 nm single-mode laser that was employed for locally illuminating a 30 µm-diameter spot on the photoanode, that was constantly polarized at an applied potential (E_{app}) of 0.85 V. Localized illumination of the surface with the invisible (for the human eye) IR laser beam induced the appearance of a bright light spot at the surface of the *n*-Si/SiO_x/Ir that could be easily observed by naked eyes and recorded with a digital camera. This PECL spot could be moved instantaneously over the photoanode surface by displacing the laser beam. This can be observed in the movie provided in Supplementary information (and the snapshots of Figure 4d) showing the displacement of the PECL spot in the photoelectrochemical cell when the incident laser spot is moved horizontally on the surface. The laser and the PECL spots could be localized and measured using a homemade hyperspectral confocal apparatus (see Methods section). As shown in Figure 4e, the excitation (i.e., the laser spot) and emission maxima (i.e., the PECL spot) are localized at the same location. These curves also show that the PECL spot size is much larger than the laser beam diameter, which is a direct consequence of the physical parameters of crystalline Si. Due to its indirect bandgap and its high charge transport capabilities, photogenerated holes have a long lifetime and a diffusion length. These results are in good agreement with the decay of the PECL profile (Figure S10), the calculation of hole diffusion length (Section 3 in Supplementary Information), and previous literature on light-addressable electrochemistry.[4,61–63]

Conclusion

Si/SiO_x/M (M = Ru, Pt, and Ir) MIS anodes were investigated for upconversion PECL of the aqueous $[Ru(bpy)_3]^{2+}$/(TPrA) model system at physiological pH. The performance of the anodes was first assessed for ECL in the dark, with non-photoactive p^{++}-Si substrates, and, then, under IR illumination, with photoactive *n*-Si substrates. We found that while Si/SiO_x/Ru fails in the anodic regime due to dramatic oxidation, Si/SiO_x/Pt and Si/SiO_x/Ir exhibit outstanding performance. Specifically, *n*-Si/SiO_x/Pt generates PECL with an unprecedented photovoltage of 480 mV and *n*-Si/SiO_x/Ir allows to generate bright PECL for 35 h. This is remarkable when considering the low stability of Si photoanodes and previous reports achieving a maximum operation time for upconversion PECL of only 15 min (Table S1).[3] This anti-Stokes PECL process allows to convert IR irradiation (λ_{exc} = 850 nm) in a visible signal (λ_{em} = 632 nm) onto the whole surface of the MIS photoanode or at a specifically-chosen location when an IR beam with a small spot size is used, which was demonstrated on proof-of-principle experiments. As the spatial resolution is mainly controlled by the high performance of crystalline Si, we anticipate that the resolution for site-selective PECL will be improved soon by semiconductor engineering. These results provide solutions to break the wall of instability, which hindered the application of PECL for technological issues and open exciting opportunities in IR imaging, (bio)analysis, and microscopy.

Acknowledgements

This work was funded by ANR (LiCORN, ANR-20-CE29-0006). Loïc Joanny and Francis Gouttefangeas from ScanMAT/CMEBA are acknowledged for SEM analyses.

Keywords: localized electrochemistry • luminescence • photoelectrochemistry • silicon • upconversion •

[1] D. Laser, A. J. Bard, *Chem. Phys. Lett.* **1975**, *34*, 605–610.

[2] J. D. Luttmer, A. J. Bard, *J. Electrochem. Soc.* **1979**, *126*, 414–419.

[3] Y. Zhao, J. Yu, G. Xu, N. Sojic, G. Loget, *J. Am. Chem. Soc.* **2019**, *141*, 13013–13016.

[4] Y. B. Vogel, N. Darwish, S. Ciampi, *Cell Rep. Phys. Sci.* **2020**, *1*, 100107.

[5] J. Yu, H. Saada, R. Abdallah, G. Loget, N. Sojic, *Angew. Chem. Int. Ed.* **2020**, *59*, 15157–15160.

[6] J. Yu, H. Saada, N. Sojic, G. Loget, *Electrochim. Acta* **2021**, *381*, 138238.

[7] Z. Liu, W. Qi, G. Xu, *Chem. Soc. Rev.* **2015**, *44*, 3117–3142.

[8] N. Sojic, *Analytical Electrogenerated Chemiluminescence: From Fundamentals to Bioassays*, The Royal Society Of Chemistry, **2020**.

[9] E. Faatz, A. Finke, H.-P. Josel, G. Prencipe, S. Quint, M. Windfuhr, in *Anal. Electrogenerated Chemilumin. From Fundam. to Bioassays*, The Royal Society Of Chemistry, **2020**, pp. 443–470.

[10] A. Zanut, A. Fiorani, S. Canola, T. Saito, N. Ziebart, S. Rapino, S. Rebeccani, A. Barbon, T. Irie, H.-P. Josel, F. Negri, M. Marcaccio, M. Windfuhr, K. Imai, G. Valenti, F. Paolucci, *Nat. Commun.* **2020**, *11*, 2668.

[11] H. Qi, C. Zhang, *Anal. Chem.* **2020**, *92*, 524–534.

[12] C. Ma, Y. Cao, X. Gou, J.-J. Zhu, *Anal. Chem.* **2020**, *92*, 431–454.

[13] J. E. Dick, C. Renault, B.-K. Kim, A. J. Bard, *Angew. Chem. Int. Ed.* **2014**, *53*, 11859–11862.

[14] M. W. Glasscott, J. E. Dick, *J. Phys. Chem. Lett.* **2020**, *11*, 4803–4808.

[15] S. Voci, B. Goudeau, G. Valenti, A. Lesch, M. Jović, S. Rapino, F. Paolucci, S. Arbault, N. Sojic, *J. Am. Chem. Soc.* **2018**, *140*, 14753–14760.

[16] W. Guo, P. Zhou, L. Sun, H. Ding, B. Su, *Angew. Chem. Int. Ed.* **2021**, *60*, 2089–2093.

[17] C. Cui, R. Jin, D. Jiang, J. Zhang, J. Zhu, *Research* **2021**, *2021*, 1742919.

[18] J. Dong, Y. Lu, Y. Xu, F. Chen, J. Yang, Y. Chen, J. Feng, *Nature* **2021**, *596*, 244–249.

[19] F. Kanoufi, N. Sojic, *Nature* **2021**, *596*, 194–195.

[20] M.-M. Chen, C.-H. Xu, W. Zhao, H.-Y. Chen, J.-J. Xu, *J. Am. Chem. Soc.* **2021**, *143*, 18511–18518.

[21] H. Ding, W. Guo, B. Su, *Angew. Chem. Int. Ed.* **2020**, *59*, 449–456.

[22] J. Zhang, R. Jin, D. Jiang, H.-Y. Chen, *J. Am. Chem. Soc.* **2019**, *141*, 10294–10299.

[23] R. A. Marcus, *J. Chem. Phys.* **1965**, *43*, 2654–2657.

[24] W. Miao, *Chem. Rev.* **2008**, *108*, 2506–2553.

[25] A. J. Bard, M. S. Wrighton, *J. Electrochem. Soc.* **1977**, *124*, 1706–1710.

[26] Y. Zhao, L. Bouffier, G. Xu, G. Loget, N. Sojic, *Chem. Sci.* **2022**, DOI 10.1039/D1SC06987J.

[27] S. Ciampi, P. K. Eggers, G. Le Saux, M. James, J. B. Harper, J. J. Gooding, *Langmuir* **2009**, *25*, 2530–2539.

[28] H. Savin, P. Repo, G. von Gastrow, P. Ortega, E. Calle, M. Garín, R. Alcubilla, *Nat. Nanotechnol.* **2015**, *10*, 624–628.

[29] G. A. Heath, T. J. Silverman, M. Kempe, M. Deceglie, D. Ravikumar, T. Remo, H. Cui, P. Sinha, C. Libby, S. Shaw, K. Komoto, K. Wambach, E. Butler, T. Barnes, A. Wade, *Nat. Energy* **2020**, *5*, 502–510.

[30] F. Priolo, T. Gregorkiewicz, M. Galli, T. F. Krauss, *Nat. Nanotech.* **2014**, *9*, 19–32.

[31] J. Wang, F. Sciarrino, A. Laing, M. G. Thompson, *Nat. Photonics* **2020**, *14*, 273–284.

[32] S. W. Boettcher, J. M. Spurgeon, M. C. Putnam, E. L. Warren, D. B. Turner-Evans, M. D. Kelzenberg, J. R. Maiolo, H. A. Atwater, N. S. Lewis, *Science* **2010**, *327*, 185–187.

[33] Z. Luo, T. Wang, J. Gong, *Chem. Soc. Rev.* **2019**, *48*, 2158–2181.

[34] S. Hu, M. R. Shaner, J. A. Beardslee, M. Lichterman, B. S. Brunschwig, N. S. Lewis, *Science* **2014**, *344*, 1005–1009.

[35] D. Bae, B. Seger, P. C. K. Vesborg, O. Hansen, I. Chorkendorff, *Chem. Soc. Rev.* **2017**, *46*, 1933–1954.

[36] K. Sun, S. Shen, Y. Liang, P. E. Burrows, S. S. Mao, D. Wang, *Chem. Rev.* **2014**, *114*, 8662–8719.

[37] X. G. Zhang, *Electrochemistry of Silicon and Its Oxide*, Kluwer Academic, **2001**.

[38] A. G. Scheuermann, J. P. Lawrence, K. W. Kemp, T. Ito, A. Walsh, C. E. D. Chidsey, P. K. Hurley, P. C. McIntyre, *Nat. Mater.* **2016**, *15*, 99.

[39] A. G. Scheuermann, K. W. Kemp, K. Tang, D. Q. Lu, P. F. Satterthwaite, T. Ito, C. E. D. Chidsey, P. C. McIntyre, *Energy Environ. Sci.* **2016**, *9*, 504–516.

[40] F. A. L. Laskowski, M. R. Nellist, R. Venkatkarthick, S. W. Boettcher, *Energy Environ. Sci.* **2017**, *10*, 570–579.

[41] I. A. Digdaya, G. W. P. Adhyaksa, B. J. Trześniewski, E. C. Garnett, W. A. Smith, *Nat. Commun.* **2017**, *8*, 15968.

[42] K. Oh, C. Mériadec, B. Lassalle-Kaiser, V. Dorcet, B. Fabre, S. Ababou-Girard, L. Joanny, F. Gouttefangeas, G. Loget, *Energy Environ. Sci.* **2018**, *11*, 2590–2599.

[43] G. Loget, *Curr. Opin. Colloid Interface Sci.* **2019**, *39*, 40–50.

[44] F. A. L. Laskowski, S. Z. Oener, M. R. Nellist, A. M. Gordon, D. C. Bain, J. L. Fehrs, S. W. Boettcher, *Nat. Mater.* **2020**, *19*, 69–76.

[45] J. R. Hemmerling, A. Mathur, S. Linic, *Acc. Chem. Res.* **2021**, *54*, 1992–2002.

[46] Y. W. Chen, J. D. Prange, S. Dühnen, Y. Park, M. Gunji, C. E. D. Chidsey, P. C. McIntyre, *Nat Mater* **2011**, *10*, 539–544.

[47] M. J. Kenney, M. Gong, Y. Li, J. Z. Wu, J. Feng, M. Lanza, H. Dai, *Science* **2013**, *342*, 836–840.

[48] J. C. Hill, A. T. Landers, J. A. Switzer, *Nat. Mater.* **2015**, *14*, 1150–1155.

[49] G. Loget, B. Fabre, S. Fryars, C. Mériadec, S. Ababou-Girard, *ACS Energy Lett.* **2017**, *2*, 569–573.

[50] G. Loget, C. Mériadec, V. Dorcet, B. Fabre, A. Vacher, S. Fryars, S. Ababou-Girard, *Nat. Commun.* **2019**, *10*, 3522.

[51] K. Oh, V. Dorcet, B. Fabre, G. Loget, *Adv. Energy Mater.* **2020**, *10*, 1902963.

[52] S. Lee, L. Ji, A. C. De Palma, E. T. Yu, *Nat. Commun.* **2021**, *12*, 3982.

[53] G. Valenti, A. Fiorani, H. Li, N. Sojic, F. Paolucci, *ChemElectroChem* **2016**, *3*, 1990–1997.

[54] R. T. Tung, *App. Phys. Rev.* **2014**, *1*, 011304.

[55] M. Pourbaix, *Atlas of Electrochemical Equilibria in Aqueous Solutions*, National Association Of Corrosion Engineers, Houston, Tex., **1974**.

[56] J. Hölzl, F. K. Schulte, in *Solid Surf. Physics. Springer Tracts Mod. Physics, Vol 85* (Eds.: J. Hölzl, F.K. Schulte, H. Wagner), Springer Berlin Heidelberg, Berlin, Heidelberg, **1979**, pp. 1–150.

[57] G. N. Derry, M. E. Kern, E. H. Worth, *J. Vac. Sci. Technol. A* **2015**, *33*, 60801.

[58] P. Aroonratsameruang, P. Pattanasattayavong, V. Dorcet, C. Mériadec, S. Ababou-Girard, S. Fryars, G. Loget, *J. Phys. Chem. C* **2020**, *124*, 25907–25916.

[59] Y. Zhao, J. Yu, J.-F. Bergamini, Y. Léger, N. Sojic, G. Loget, *Cell Rep. Phys. Sci.* **2021**, 100670.

[60] D. Han, B. Goudeau, D. Jiang, D. Fang, N. Sojic, *Anal. Chem.* **2021**, *93*, 1652–1657.

[61] H. Zhu, B. Miller, D. Scherson, *J. Electrochem. Soc.* **2010**, *157*, F137.

[62] M. H. Choudhury, S. Ciampi, Y. Yang, R. Tavallaie, Y. Zhu, L. Zarei, V. R. Gonçales, J. J. Gooding, *Chem. Sci.* **2015**, *6*, 6769–6776.

[63] Y. B. Vogel, J. J. Gooding, S. Ciampi, *Chem. Soc. Rev.* **2019**, *48*, 3723–3739.

Entry for the Table of Contents

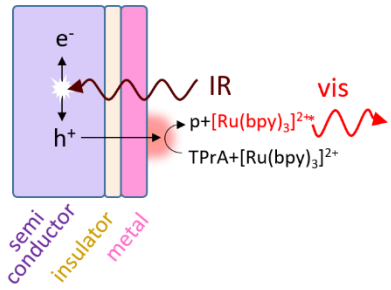

n-Si/SiO_x/Pt and *n*-Si/SiO_x/Ir exhibit high photovoltages and record stabilities in operation (up to 35 h) for the generation of intense anti-Stokes photoinduced electrochemiluminescence onto the whole surface of the MIS photoanode or at a specifically-chosen location. These results provide solutions for overcoming the instability that has hampered the practical application of upconversion PECL.

Institute and/or researcher Twitter usernames: @chimie_ISCR